Enhanced DySEM imaging of cantilever motion using artificial structures patterned by focused ion beam techniques

OPEN ACCESS
IOP Publishing
Journal of Micromechanics and Microengineering
J. Micromech. Microeng. **26** (2016) 035010 (7pp)
doi:10.1088/0960-1317/26/3/035010

Enhanced DySEM imaging of cantilever motion using artificial structures patterned by focused ion beam techniques

M-A Schröter[1], M Ritter[2], M Holschneider[3] and H Sturm[1,4]

[1] Bundesanstalt für Materialforschung und -prüfung (BAM), D-12205 Berlin, Germany
[2] Electron Microscopy Unit, Hamburg University of Technology, D-21073 Hamburg, Germany
[3] Department of Mathematics, University of Potsdam, D-14469 Potsdam, Germany
[4] Technische Universität Berlin, D-10587 Berlin, Germany

E-mail: maria-astrid.schroeter@bam.de

Received 4 November 2015, revised 9 December 2015
Accepted for publication 21 December 2015
Published 4 February 2016

Abstract

We use a dynamic scanning electron microscope (DySEM) to map the spatial distribution of the vibration of a cantilever beam. The DySEM measurements are based on variations of the local secondary electron signal within the imaging electron beam diameter during an oscillation period of the cantilever. For this reason, the surface of a cantilever without topography or material variation does not allow any conclusions about the spatial distribution of vibration due to a lack of dynamic contrast. In order to overcome this limitation, artificial structures were added at defined positions on the cantilever surface using focused ion beam lithography patterning. The DySEM signal of such high-contrast structures is strongly improved, hence information about the surface vibration becomes accessible. Simulations of images of the vibrating cantilever have also been performed. The results of the simulation are in good agreement with the experimental images.

Keywords: FIB patterning, structured cantilever, AFM, modal analysis, DySEM

(Some figures may appear in colour only in the online journal)

1. Introduction

The progressing miniaturization of technical applications leads to a growing interest in imaging techniques with high resolution. Micro- and nano-electromechanical systems (MEMS/NEMS), for example, are an indispensable technical basis for modern innovative solutions. Their functionality is often based on mirrors, switches, resonators and generally on oscillatory systems at the micro- and nano-scale.

Cantilevers, clamped at one side, are such oscillatory systems. The use of cantilevers with different geometries has been limited for a long time to atomic force microscopy (AFM). In recent years, numerous other applications have opened up which exploit the versatile sensor properties of cantilevers. In this case, the basic principle consists in the conversion of a physical information contained in a mechanical signal [1, 2], i.e. a change of frequency, phase or amplitude as well as in the most general form a quasi-static cantilever bending. For example, the adhesion of a particle with a certain mass on the lever will result in a low-frequency shift of the resonance frequency and, additionally, to beam bending. This frequency shift is a function of the position of the applied mass along the cantilever [3–5]. Hence, the large number of such signals that can be detected has led to a rapid development of these sensoring techniques in the field of medical technology, environmental pollution control (*chemical nose*) [6] and monitoring of industrial manufacturing processes.

In the simplest case the flexural vibration of a cantilever can be described with the Euler–Bernoulli equation [7–10]. This equation is based on the approximation of a thin plate. The mass of the tip at the very end of the cantilever is neglected. The cantilever is considered to be a beam of constant cross-section, which

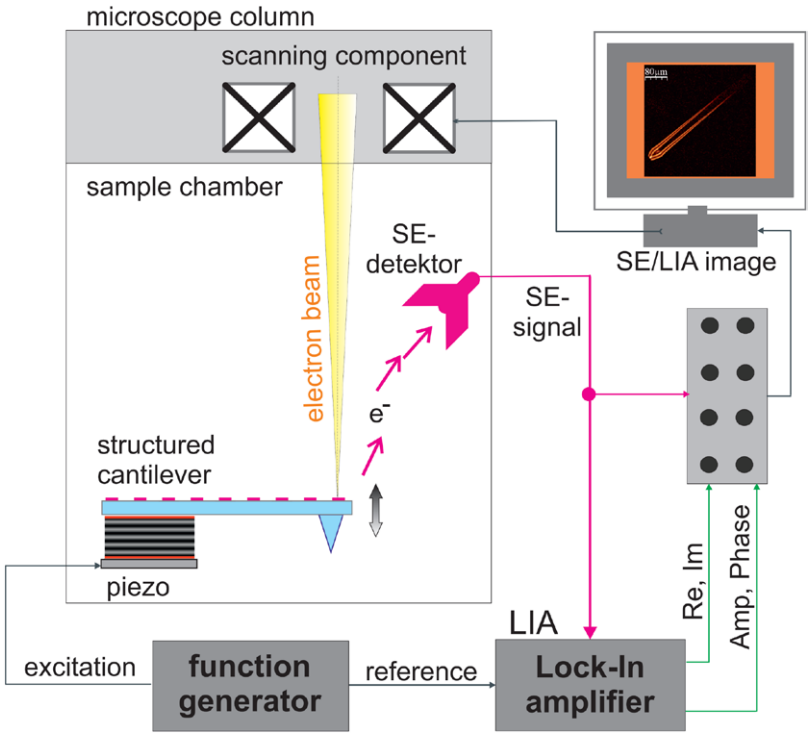

Figure 1. The DySEM technique: experimental setup.

is always oriented perpendicular to the beam axis. Additionally, the dimensions of the cantilever (length, width and thickness) are much larger than both the characteristic microscopic lengths (e.g. lattice constant) and the deflection of the beam itself. Like the Timoshenko beam theory, the Euler–Bernoulli equation permits the calculation of cantilever deflections and of the precise position of the vibrational nodes. Yet shear deformations, which are accounted for in Timoshenko theory, are neglected by the Euler–Bernoulli theory.

Although an optimization of design parameters or failure tracking for these kinds of micro- and nanobeams can often be obtained only by imaging the vibration, finite element methods [11, 12] or other sophisticated numerical techniques yield good numerical results [13]. However, these predictions and calculations for the vibrational behaviour of resonant structures require experimental input parameters. In particular, for AFM probes or for cantilever-based sensors, a precise control of vibration shape, frequency and amplitude is indispensable.

Classically, the imaging of vibrating microscale structures is performed by scanning interferometric techniques. However, a critical limitation is the lack of high-sensitivity position detection mechanisms for small structures according to the law of Abbe. During the last few years, techniques such as stimulated emission depletion microscopy (STED) [14], techniques using laser light scattering [15], scanning nearfield optical microscopy (SNOM) [16], and the use of an electron beam with its much smaller beam diameter (compared to a laser spot) were successfully applied to overcome this limitation.

In this paper, imaging of the cantilever vibration is achieved *in situ* by an electron beam and lock-in technology. This technique is called *dynamic scanning electron microscopy* (DySEM). The DySEM technique allows measurements of vibrating micro- and nano-structures at different resonance modes and even at higher harmonics. Here, the imaging process is based on a modulation of secondary electron (SE) signal at a given electron beam position due to a local contrast variation on the cantilever. For this reason, a flat surface of a cantilever with no material contrast is not sensitive to this technique, and only the edges and the very end of the lever lead to an image contrast. For many applications this is not sufficient.

In this paper we use high-contrast, circular shaped structures to obtain information of the whole cantilever surface. This is particularly useful if, for example, due to the attachment of mass [17–20] or due to contact of the cantilever tip with a surface, deviations from the conventional vibration patterns are expected. In such cases, the precise knowledge of time-varying spatial distribution of vibration displacement is important for the interpretation of every cantilever-based sensor [12, 21].

2. Experimental details

2.1. DySEM technique

The DySEM measurements were performed as described in [22, 23]; so the setup here is described again only briefly.

In a DySEM measurement the oscillation of a cantilever is imaged by the use of an electron beam. The vibration of the cantilever is excited by a piezoelectric ceramic at its base, driven by a function generator (figure 1). If the driving frequency is close to the resonance frequency, excitation of the cantilever occurs. The dynamic response of the vibrating cantilever is measured using secondary electron detector signals (SE

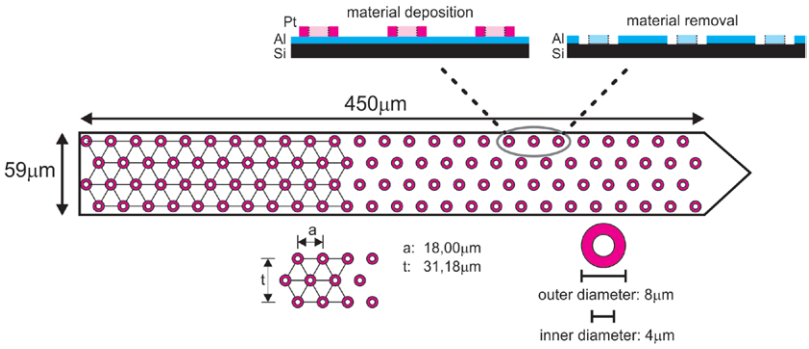

Figure 2. Scheme of structured cantilever with marked positions for the circular shaped material deposition and removal, respectively (top view). The marks are at positions of a triangular lattice.

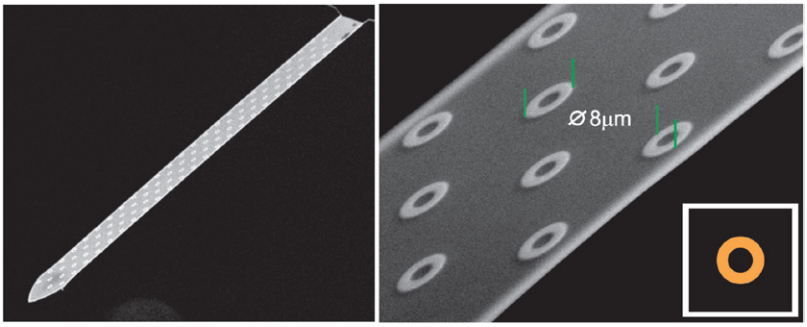

Figure 3. Circular shaped material deposition, overview (left) and zoom (right). The cantilever is tilted, thus structures appear distorted in this perspective. The ratio of outer to inner diameter is 2:1 as shown in the inset. Cantilever imaged at 15 kV, fixation at top right position (left image) [25].

image). In addition, the voltage proportional to the SE signal is also analyzed with the help of lock-in amplifiers synchronized to the excitation frequency (reference). The corresponding amplitude and phase values or real and imaginary parts are recorded and displayed as an image (Lock-In amplifier/LIA image). Alternatively, the signal components of integer multiples of the excitation frequency (harmonics) can be used for imaging. This leads to a sequence of images denoted with an index n.

2.2. Microstructured Cantilever

As described above, the measurements in DySEM mode are based on dynamic contrast, initiated either by a topography or by a material variation, within the electron beam diameter. For a homogeneous flat cantilever such DySEM contrast only appears at the edges.

In order to circumvent this obstacle, a cantilever[5] surface was microstructured with high-contrast structures. Circular shaped structures at defined positions were patterned on the surface of the cantilever, using focused ion beam (FIB) milling and gas-induced platinum deposition (Helios Nanolab 600, FEI, Eindhoven, The Netherlands). The reason for using rings is that they are as symmetric as circles and they give inside a second source of contrast. Modifications of cantilevers using additional masses at different positions were already calculated [17] and performed [24], however with much more simple geometries.

The circular rings are positioned on the cantilever surface at the corners of a triangular lattice (figure 2). The outer rings are written as close as possible to the edge lines, but without overlapping or being incomplete. Furthermore, disruption of the cantilever during lithographic milling as well as supernatant deposition should be avoided.

To define the optimal distance between the circular rings a compromise had to be made. On the one hand, a grid of small structures as dense as possible is useful to achieve high resolution. On the other hand, at high excitation amplitudes a signal overlapping during DySEM occurs in case of a high density of structures.

In addition, a cantilever structured in this way is symmetric, which is necessary to perform an analysis using the Euler–Bernoulli equation. Therefore, as expected and intended, no deviations from the modal deflection of an unmarked cantilever in our measurements can be found. Obviously, all structures either increase (deposition) or decrease (milling) the local mass and complementarily also change local cantilever stiffness [12]. This will be addressed in detail in a following paper.

When the cantilever is tilted (figure 3), the change in aspect ratio of the circles can be corrected by expansion or

[5] Silicon contact cantilever type PPP-CONTR from Nanosensors, Neuchâtel, Switzerland. Geometry: rectangular, length: 447 μm, width: 58–60 μm, height: 1.4–2.0 μm. Covered with 30 nm aluminium.

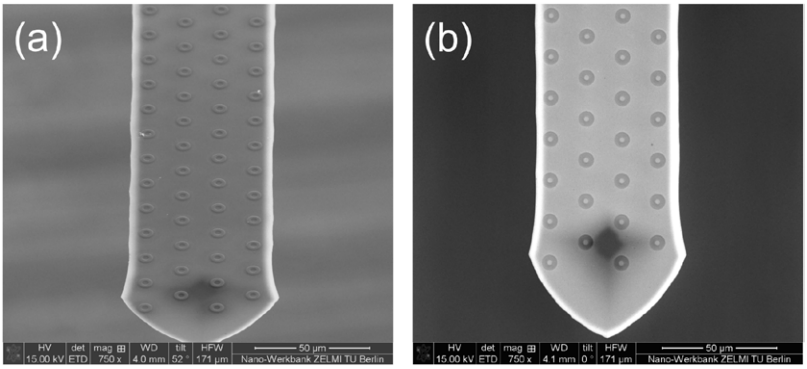

Figure 4. Structured cantilever of type *PPP-CONTR*[6]. (a): Deposited platinum rings on the aluminized surface of the cantilever. Material deposition (estimated): 50–100 nm. (b): In the aluminium-coating etched concentric rings. The material removal is between 30 and 60 nm (estimated) [25].

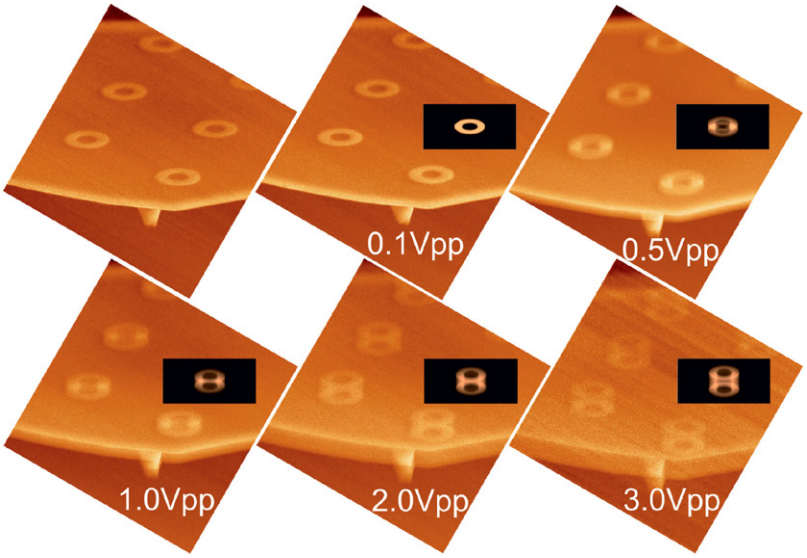

Figure 5. *SE*-micrographs of the first flexural mode (*T-B* #1). Amplitude-dependent transformation of the circular structure (top row, left: no excitation). The inset in the figures shows the simulated structure. Imaged at 15 kV.

compression of the projection distortion. However, the rotation of the cantilever plane below the electron beam was not reconstructed and is not a topic of this paper. For such purposes the triangular superstructure of the positions of circles could be used.

Two different types of modified cantilevers have been produced (figure 4): cantilevers with raised rings of platinum (a) and cantilevers with rings etched into the aluminium coated surface (b). In this paper we present measurements performed with the cantilever deposited platinum rings.

Due to the fact that the mass of the Pt structures or the loss of mass for the etched structures are in total about 0.3 ng (Pt) and 0.02 ng (Al) compared to the mass of cantilever of about 110 ng, the influence on the vibration is neglected at this time. Further experiments are planned to deposit or remove small masses during vibration to demonstrate that DySEM is sufficiently sensitive to compare these two cases. As of this point in time, the variation due to changes within the commercial cantilevers are definitively higher than the influence of the discussed mass changes, so unfortunately up to now experiments clarifying this situation have not been possible.

3. Results and discussion

3.1. Spatially resolved measurements

In figure 5 the conventional SE contrast of the structured cantilever excited at its first flexural resonance mode (*T-B*#1 at 8.999, 5 Hz) is shown. The cantilever is imaged at its freely moving end, and the tip is clearly visible. The excitation amplitude varies between 0.1 and 3 Vpp. If the oscillation amplitude increases, the topology of the circular rings changes. Starting from a simple blurring in the form of a halo, the structures gain a more and more complicated form. This is due to an interaction phenomenon of overlapping edges. This result is in agreement with the simulation, shown as an inset in each figure. The simulated images are obtained by numerical integration of imaging equations [22], yielding the SE signal for each point of the cantilever surface.

[6] See footnote 5.

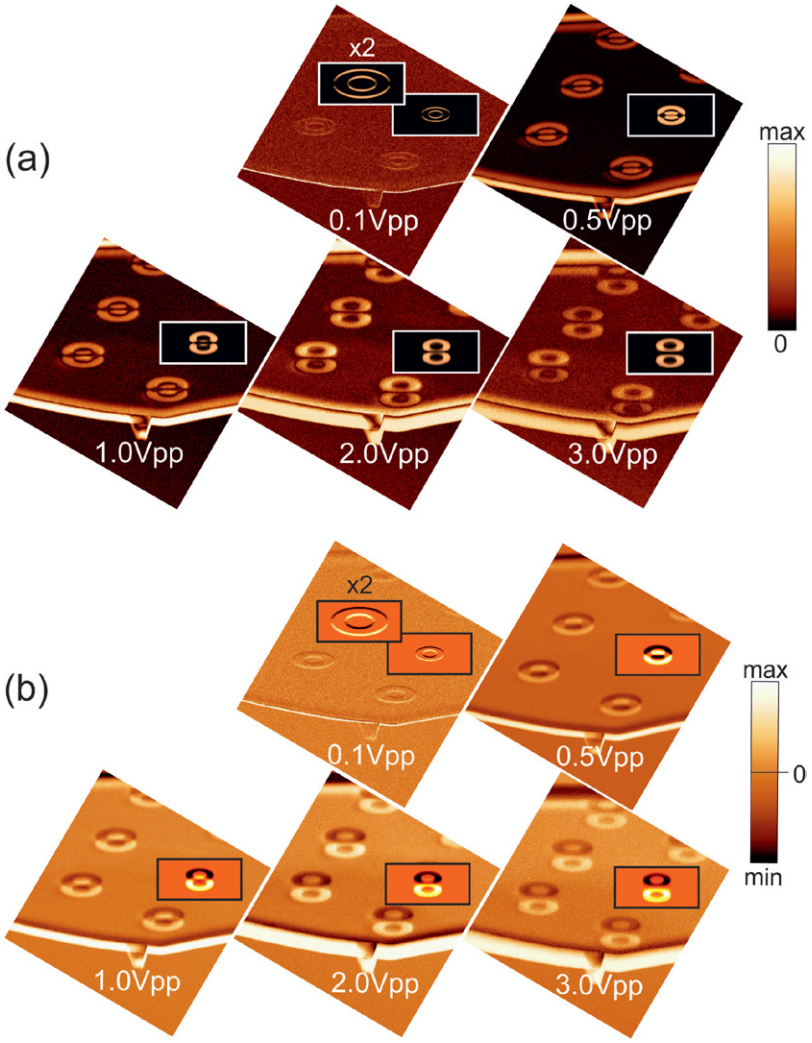

Figure 6. First flexural mode (*T-B*#1, $n = 1$): *LIA*-amplitude (a) and *LIA*-real part (b). The inset in the images shows the simulated circular structure.

In the corresponding LIA images (figure 6), the local distribution of reference synchronous vibration components of the cantilever is shown. The amplitude images are shown in (a) and the real part images in (b). The colour coding corresponds to the lock-in amplifier output voltages.

The amplitude images are each normalized and show the distribution of absolute values. The scale ranges from black (no signal) to white (maximum). At a low excitation amplitude the surface of the cantilever is free of contrast; only at the cantilever edges and at the boundary of the artificial structures a contrast appears. Increasing the excitation amplitude a figure similar to an analemma appears.

As discussed in a recent work [23], the LIA imaginary part as a measure of energy loss per cantilever oscillation is close to zero, so that only real part images are informative. This is due to the imaging in high vacuum. Therefore, in the complex plane, the corresponding phase values are given either by 0° or 180°. Thus, a change of sign in real part contrast is always correlated with a phase shift. Therefore, in contrast to the amplitude images, the colour range of real part images (figure 6(b)) varies from black (minimum) to white (maximum) including a change of sign.

In the case of any artificial damping the imaginary part will contain a second piece of information in form of a new contrast, physically independent from the real part image.

Figure 7 shows the SE image and two harmonics ($n = 1, 2$) of the second flexural mode (*T-B*#2 at 57.246 Hz). The excitation amplitude is fixed at 2 Vpp. The position of the vibration node is clearly visible by the interruption of the edge line in the LIA images due to a lack of dynamic contrast. Circular shaped structures, which are located at the vibration node, do not blur in the SE image; whereas in the LIA images the structures vanish, because there is no modulation of the SE yield at this position. At the very end of the cantilever the deflection is high and the marks are getting from the node line to the freely moving end more and more blurred. Additionally, the splitting of the edge line in a doublet can be observed for $n = 2$ as described in detail theoretically in [23].

A similar result can be observed in figure 8 for the first torsional mode (*L-R*#1 at 132.083 Hz). The excitation amplitude is fixed at 4 Vpp. Structures at the symmetry axis yield no information, since they are located at the vibration node. The nodes are clearly visible in the images. They correspond to zones of absence of motion and therefore the local image

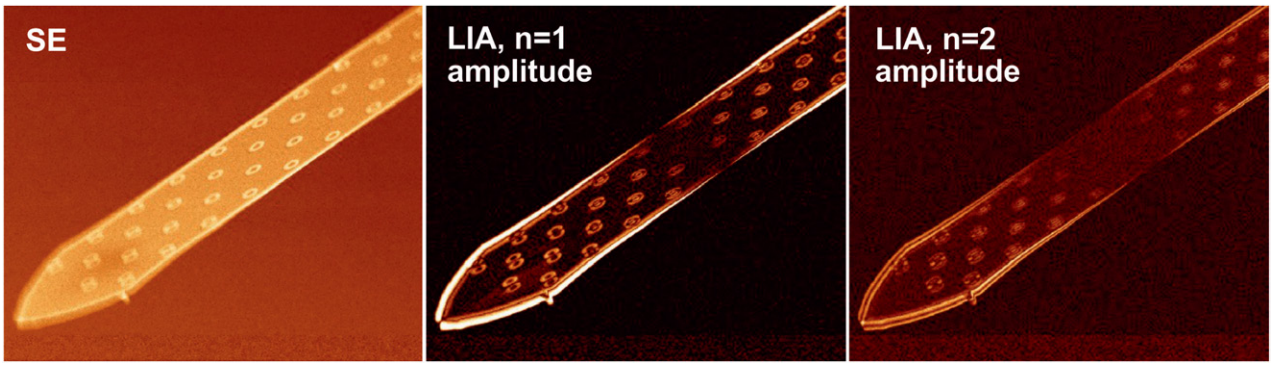

Figure 7. Oscillating cantilever at the second flexural mode (*T-B*#2). Lithographed structures that are located at the vibration node do not blur. At the very end of the cantilever, the deviation from the circular structure is high. *SE* image at 15 kV.

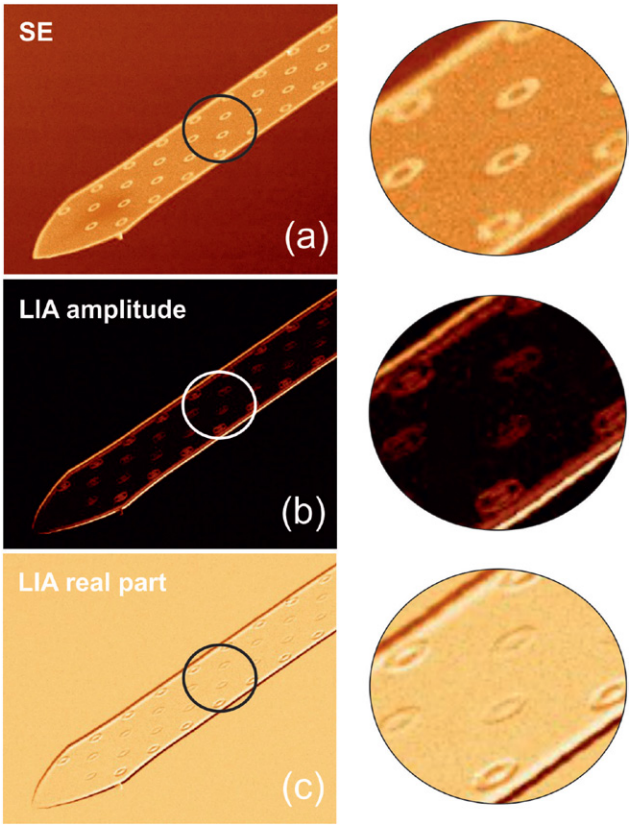

Figure 8. First torsional mode (*L-R*#1, $n = 1$): *SE*-micrograph (a), *LIA*-amplitude (b), *LIA*-real part (c). The mapping of local blurring at the position of the circular structures allows the reconstruction of the vibration [25]. *SE* image at 15 kV.

corresponds to the static image. With increasing distance from the vibration node, blurring enlarges towards the edges (a).

As described below, the visibility and the shape of the structures in the LIA images depend on the modulation of the SE yield. For this reason, the side of the circular structures oriented towards the vibration node is hardly visible, whereas the visibility increases towards the edges ((b), (c)). Also, the very end of the cantilever, intersected by the nodal line, is not visible. It can be concluded that the LIA imaging is more sensitive to the vibration than the SE mapping.

Theoretical considerations

The derivation of the DySEM-imaging equations is described in [22, 23].

Briefly summarized, the interaction of the periodically bending cantilever with the electron beam is described by an angle- and time-dependent distribution of emitted electrons. However, the scattering distribution is also a function of cantilever material and topography. At positions without any contrast, the SE signal stays constant, despite the fact that the cantilever oscillates within the electron beam. Hence, the LIA-signal, which is sensitive to the dynamic SE contrast, vanishes at these positions.

Due to the cantilever vibration the instantaneous intersection point of the electron beam with the cantilever surface is time-variable during an oscillation period. For this reason, the electron beam describes a curve (trajectory) on the cantilever surface. Since the direction of the incoming electron beam related to the cantilever is fixed, the length of this trajectory is only determined by the local oscillation amplitude at the particular cantilever position.

Therefore, a modulation of the SE-signal at a cantilever position occurs, when the intensity of the detected scattered electrons changes along the electron beam trajectory. For a homogeneous flat cantilever this is generally the case at positions with local contrast variation of the sample, in particular at the edge of the cantilever towards the non-emitting background out of focus.

The derived DySEM imaging equations consist mainly of two parts: a function describing the cantilever material (contrast) and kernel functions modifying the local scattering distribution. Since the kernel functions are scaled by the length of the electron trajectory, the modification of the scattering function is locally different. So, it can be concluded that each pixel of the SE and LIA-image is assigned by the value, which results from the scalar product of the material contrast function with the kernel function shifted to that location and scaled by the local amplitude of oscillation.

Based on the Euler–Bernoulli equation results for the flexural oscillation can be simulated. Neglecting cantilever modifications like the tip or the triangular shape at the very end of the lever the equation is valid for small beam deflection. The instantaneous intersection point of the electron beam with the lever was computed using an iterative numerical

method. So, the time-variable density of emitted electrons was decomposed to the individual LIA components using discrete Fourier transformation. Hence, the signal for the total intensity corresponds to the zeroth Fourier mode (SE image). The SE/LIA images are then calculated by the numerical integration of imaging equations.

4. Conclusion

In this paper we demonstrate the use of artificial, high-contrast structures on vibrating cantilevers in DySEM imaging techniques. We could by these means resolve the local vibrational amplitude and phase distribution over the vibrating structure. Such imaging of structures on cantilevers could be useful if local loads such as particles or cells need to be detected using a frequency analysis of a specific mode. As proven by Dohn *et al* [4], only the deflected parts of a vibrating lever contribute to the resonance shift that can be used for mass detection. In addition, resonance measurements of vibrating levers with attached structures of higher aspect ratio are found to also be sensitive to the orientation of the attached particle related to the lever [12]. Therefore, not only the sensitivity of a cantilever mass detector changes with the position of the adsorbate, but the whole resonance behaviour in thr form of the dynamic lever shape. Thus, reliable and reproducible measurements based on this technique will need a DySEM analysis of the mode shape behaviour with and without the attachments. Techniques like FAM-AFM [26] or dual-frequency AFM [27] as well as experiments with mixed flexural and torsional modes should profit by a detailed imaging of vibrating cantilevers using DySEM.

Acknowledgments

We want to thank D Berger (ZELMI, TU Berlin) for his support with the FIB milling and the platinum deposition.

References

[1] Raiteri R, Grattarola M, Butt H-J and Skládal P 2001 *Sensors Actuators* B **79** 115–26
[2] Lavrik N V, Sepaniak M L and Datskos P G 2004 *Rev. Sci. Instrum.* **75** 2229–53
[3] Ramos D, Tamayo J, Mertens J, Calleja M, Villanueva L G and Zaballos A 2008 *Nanotechnology* **19** 035503
[4] Dohn S, Sandberg R, Svendsen W and Boisen A 2005 *Appl. Phys. Lett.* **86** 233501
[5] Dohn S, Schmid S, Amiot F and Boisen A 2010 *Appl. Phys. Lett.* **97** 044103
[6] Fadel L, Lochon F, Dufour I and Français O 2004 *J. Micromech. Microeng.* **14** 23–30
[7] Meirovitch L 1985 *Elements of Vibration Analysis* (New York: McGraw-Hill)
[8] Morse P M and Ingard K U 1986 *Theoretical Acoustics* (New York: McGraw-Hill)
[9] Stokey W F 1976 *Shock, Vibration Handbook* (New York: McGraw-Hill)
[10] Rayleigh J W S and Lindsay R B 1945 *The Theory of Sound (Dover Classics of Science & Mathematics)* (New York: Dover)
[11] Song Y X and Bhushan B 2006 *Ultramicroscopy* **106** 847–73
[12] Ruz J J, Tamayo J, Pini V, Kosaka P M and Calleja M 2014 *Sci. Rep.* **4** 6051
[13] Raman A, Melcher J and Tung R 2008 *Nano. Today* **3** 20–7
[14] Klar T A, Jakobs S, Dyba M, Egner A and Hell S W 2000 *P. Natl Acad. Sci. USA* **97** 8206–10
[15] Sanii B and Ashby P D 2010 *Phys. Rev. Lett.* **104** 147203
[16] Heinzelmann H and Pohl D W 1994 *Appl. Phys.* A **59** 89–101
[17] Li H, Chen Y and Dai L 2008 *Appl. Phys. Lett.* **92** 151903
[18] Bowen J, Cheneler D, Walliman D, Arkless S, Zhang Z, Ward M C L and Adams M J 2010 *Meas. Sci. Technol.* **21** 115106
[19] Joachim D and Lin L 2003 *J. Microelectromech. Syst.* **12** 193–200
[20] Gil-Santos E, Ramos D, Martinez J, Fernandez-Regulez M, Garcia R, San Paulo A, Calleja M and Tamayo J 2010 *Nat. Nanotechnol.* **5** 641–5
[21] Tamayo J, Kosaka P M, Ruz J J, San Paulo A and Calleja M 2013 *Chem. Soc. Rev.* **42** 1287–311
[22] Schröter M A, Holschneider M and Sturm H 2012 *Nanotechnology* **23** 435501
[23] Schröter M A, Sturm H and Holschneider M 2013 *Nanotechnology* **24** 215701
[24] Enderling S, Hedley J, Jiang L, Cheung R, Zorman C, Mehregany M and Walton A J 2007 *J. Micromech. Microeng.* **17** 213–9
[25] Schröter M-A 2014 *PhD Thesis* Berlin (https://opus4.kobv.de/opus4-tuberlin/files/5883/schroeter_maria_astrid.pdf)
[26] Solares S D 2007 *Meas. Sci. Technol.* **18** 592–600
[27] Chawla G and Solares S D 2009 *Meas. Sci. Technol.* **20** 015501